Spatio-temporal variability of surface mass balance in the accumulation zone of the Mer de Glace, French Alps, from multitemporal terrestrial LiDAR measurements

Marion Réveillet* [iD], Christian Vincent [iD], Delphine Six [iD], Antoine Rabatel [iD], Olivier Sanchez, Luc Piard and Olivier Laarman

Univ. Grenoble Alpes, CNRS, IRD, Institut des Géosciences de l'Environnement (IGE, UMR 5001), Grenoble 38000, France

Abstract

Spatio-temporal variability of the winter surface mass balance is a major uncertainty in the modelling of annual surface mass balance. Moreover, its measurement at high spatio-temporal resolution (sub-200 m) is very useful to force, calibrate or validate models. This study presents the results of year-round field campaigns to study the evolution of the surface mass balance in a $\sim$2 km^2 portion of the accumulation zone of the Mer de Glace (France). It is based on repeated LiDAR acquisitions, submergence-velocity measurements and meteorological records. The two methods used to quantify submergence velocities show good agreement. They present a linear temporal evolution without significant seasonal changes but display significant spatial variability. We conclude that a dense network of submergence velocity measurements is required to reduce the uncertainties when computing winter and annual surface mass balance from digital elevation model differencing. Finally, a hight spatio-temporal variability of the winter surface mass balance is highlighted (e.g., a std dev. of 0.92 m in April) even though the topography is homogeneous (std dev. of 25 m). Attempts to relate this variability to different morpho-topographic variables and wind-related indexes show the need for studies conducted at the snowfall event scale to obtain a better understanding of the variability in mass balance at the glacier scale.

1. Introduction

The long-term evolution of glacier surface mass balance is known to be a very good indicator of changing climate conditions (e.g., Haeberli and Beniston, 1998; Solomon and others, 2007). In the Alps, the interannual variability of the annual surface mass balance is mainly driven by the summer surface mass balance variability (e.g., Braithwaite and Zhang, 2000; Oerlemans and Reichert, 2000; Kuhn, 2003; Six and Vincent, 2014; Davaze and others, 2020). Consequently, many studies have focused on summer surface mass-balance modelling using approaches of varying complexity (e.g., Hock, 1999; Pellicciotti and others, 2005; Gabbi and others, 2014; Réveillet and others, 2017). Nevertheless, some studies have pointed out a strong sensitivity of annual to winter surface mass balance given that the thicker the winter snowpack, the later the snow/ice transition at the glacier surface, resulting in reduced summer ablation (e.g., Paul and others, 2004; Machguth and others, 2006; Dadic and others, 2010; Réveillet and others, 2017, 2018). In addition, accumulation is considered to be the variable with the highest uncertainty in glacier surface mass-balance modelling. Therefore, assessing the spatio-temporal variability of the winter surface mass balance is important to model the annual surface mass-balance evolution with reduced uncertainties.

Snow-accumulation measurements at high resolution are very useful to force, calibrate or validate models. Complex models such as SnowTran-3D (Liston and Sturm, 1998) have been developed to simulate wind transport and have been successfully used in alpine regions (e.g., Bruland and others, 2004), but require high spatial and temporal resolution of the meteorological forcing data, as well as a good understanding of the processes responsible for snow-accumulation spatial variability (Trujillo and Lehning, 2015). Indeed, the spatio-temporal variability of winter surface mass balance due to orographic and wind effects (transport, deposition, erosion) is difficult to quantify and consequently to model at the glacier scale because in situ measurements are commonly limited to a few points per km^2 (WGMS, 2013) and may not fully represent the local effects. Indeed, while the interannual variability of precipitation amount is known to control the interannual variability of winter surface mass balance (e.g., Vincent, 2002), the topography and wind effects impact its spatial variability. Many studies have pointed out the increase in winter surface mass balance with elevation (e.g., Rohrer and others, 1994; López-Moreno and Stähli, 2008; Grünewald and Lehning, 2011; Grünewald and others, 2013; Pulwicki and others, 2018) and the amount of snow is usually assessed using a correction factor depending on elevation and a temperature threshold to characterize the precipitation phase (Vincent and others, 1997, 2007a; Hock, 1999; Machguth and others, 2006, 2009; Rabatel and others, 2008). However, the correction factor needs to be adjusted (e.g., Huss and Bauder, 2009), which requires spatialized measurements to account

for the spatial variability of winter surface mass balance in relation to processes linked with the deposition or redistribution of snow (e.g., Gerbaux and others, 2005).

Different methods can be used to measure the spatial variability of winter surface mass balance at high spatial resolution. Indeed, stakes or drilling cores provide only local information (e.g., Cogley and others, 2011). Ground-penetrating radar (GPR) can be used to determine annual snow-layer thickness over different transects (e.g., Dunse and others, 2009; Heilig and others, 2010; Helfricht and others, 2012; Sold and others, 2013). More recently, innovative techniques such as drone photogrammetry (e.g., Bühler and others, 2016), Pléiades imagery at high resolution (e.g., Marti and others, 2016) or LiDAR (Light Detection And Ranging) have been widely used on ice-free surfaces and make it possible to determine the spatial distribution of the winter surface mass balance using digital elevation model (DEM) differencing. Airborne LiDAR acquisitions provide measurements over large areas (e.g., Baltsavias, 1999; Wehr and Lohr, 1999; Lutz and others, 2003; Helfricht and others, 2012). Terrestrial LiDAR measurements generally cover smaller areas, but offer higher temporal acquisition frequencies (e.g., Prokop, 2008; Fischer and others, 2016). Nevertheless, LiDAR measurements are generally combined with other approaches to evaluate or quantify the uncertainty. For instance, Piermattei and others (2015, 2016) combined photogrammetric methods with airborne or terrestrial laser scanning, Carturan and others (2013) compared terrestrial laser surveys with a combination of geomorphological, geophysical and high-resolution geodetic surveying, and Fischer and others (2016) evaluated the airborne LiDAR measurements using in situ observations. In addition, many LiDAR measurements have been carried out on non-glacial environments to study the spatio-temporal variability of snow accumulation (e.g., Fassnacht and Deems, 2006; Trujillo and others, 2007; Grunewald and others, 2010; Grünewald and others, 2013; Kirchner and others, 2014; Revuelto and others, 2014).

Few studies have been carried out on glaciers (e.g., Deems and others, 2013; Sold and others, 2013; Gabbud and others, 2015) because of the complexity of taking into account the glacier flow and snow/firn densification. Indeed, glacier surface evolution is related to snow-accumulation changes and to submergence/emergence velocities, which can be of the same order of magnitude (e.g., Vincent and others, 2007b). Therefore, methods based on DEM comparison need to take into account the effects of glacier dynamics to quantify the surface mass balance. For this purpose, some studies have used empirical methods to estimate the vertical variations of the glacier surface topography due to ice flow (e.g., Sold and others, 2013; Schöber and others, 2014) or have used stakes to directly measure the emergence velocities at some points (e.g., Vincent and others, 1997, 2007b). The emergence velocities can be calculated from horizontal and vertical velocities and the slope of the surface. In the accumulation zone, the emergence velocities are negative (therefore called submergence), which corresponds to a downward flow of the mass relative to the glacier surface. The submergence velocity allows the surface mass balance to be related to thickness changes (Cuffey and Paterson, 2010) but is the subject of only a few studies (e.g., Vincent and others, 1997, 2007b; Kääb and Funk, 1999).

Regarding the glaciers located in the French Alps and monitored within the framework of the GLACIOCLIM (les GLACIers, un Observatoire du CLIMat) observatory (part of the French Research Infrastructure OZCAR, Gaillardet and others, 2018), the winter surface mass balance is currently measured at distinct points using the glaciological method (core drilling and density measurements). Based on these data, previous studies have shown a significant correlation between the temporal variability of precipitation and winter surface mass balance (e.g., Vincent, 2002; Six and

Vincent, 2014; Réveillet and others, 2017). However, no significant relationship between winter surface mass-balance spatial variability and topographic variables has been found (Réveillet and others, 2017). This might be due to the low spatial density of in situ measurements that does not allow local effects responsible for spatial variability over short distances to be considered (e.g., Fassnacht and Deems, 2006; López-Moreno and others, 2011). In such a context, the aim of this paper is to study the spatio-temporal evolution of surface mass balance over one year in the accumulation zone of the Mer de Glace (Mont-Blanc range, France) using repeated in situ high-resolution topographic and meteorological measurements. For that purpose, repeated LiDAR acquisitions, submergence velocity estimates and meteorological records from an automatic weather station (AWS) were collected over a one-year period. First, the experimental method will be presented along with a comparison of two methods to quantify the submergence velocities. Second, we will analyze and discuss the pattern of the spatio-temporal variability of the surface mass balance.

2. Study area

The study site is a ∼2 km^2 area located in the accumulation zone of the Mer de Glace, at the Col du Midi (45.51°N, 6.54°E, Fig. 1). This site is easily accessible by the Aiguille du Midi cable car. The area includes a small elevation range (from 3350 to ∼3600 m a.s.l.) and is relatively flat (average slope of 2°, with a maximum of 11°). The mean winter surface mass balance computed over the last 20 years, based on measurements performed at two sites following the glaciological method, is 2.2 m w.e. a^{-1} (GLACIOCLIM program). Regarding weather conditions, this area is exposed to strong north-westerly winds, mainly due to the presence of the Col du Midi pass (Météo France data).

3. Method and data

The field campaigns were conducted approximately every 5 weeks over one year, from October 2014 to October 2015. For the sake of clarity, in the following, the time period between the first campaign considered as the reference (i.e., October 2014) and a given campaign is called the total period (noted Pi, with i ∈ [1; 7]); and the time period between two successive campaigns is called a sub-period (noted SPi, with i ∈ [1; 7]). This is illustrated in Figure 2.

3.1 Terrestrial laser-scanner measurements

Terrestrial laser scanners emit laser signals and measure the return time of the signal after reflection on the scanned surface. In this study, we used an Optech ILRIS-LR long-range Terrestrial Laser Scanner (with a near-infrared wavelength of 1064 nm suited to a snow-covered surface), providing measurements over a maximum distance of 3 km. At our study site, the scanned distances range from 400 to 1800 m. Note that the beam size is 27 ± 7 mm at 100 m and increases with distance.

Over the one year study period from 31 October 2014 to 23 October 2015, eight LiDAR acquisitions were performed (see Table 1). Measurements were made from the southernmost Aiguille du Midi platform (Figs 1b, c), at the same place for each acquisition. Given the large area scanned, three scan windows were necessary to cover the entire zone. Data acquisition was made with an averaged sampling step of 0.20 m at 900 m (ranging from 0.10 to 0.42 m depending on the distance). The data obtained from the LiDAR scanner consist of point clouds that were subsequently processed with Polyworks software to obtain a DEM for each survey. First, the point clouds from the three scanned windows were aligned together. For that purpose, the least square method was applied in the overlapping areas between the different windows. Once aligned, the point clouds were
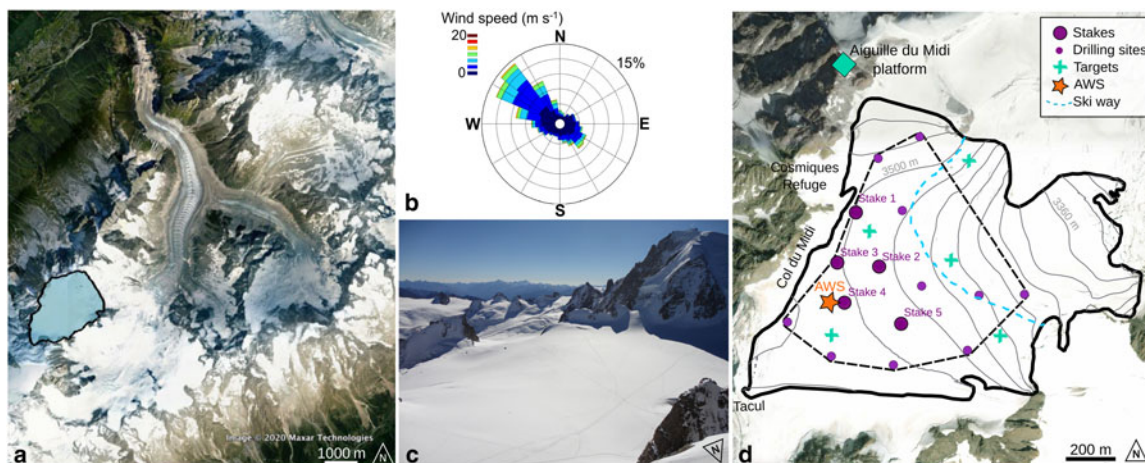
Fig. 1. (a) Location of the study site (blue area) in the Mer de Glace catchment (background image from Google Earth). (b) Wind rose from the half-hourly mean measurements at the weather station, indicated with an orange star on (d), over the period February–October 2015. (c) Photograph of the study area taken on 31 October 2014 from the Aiguille du Midi platform where the terrestrial LiDAR was set up, indicated by a green diamond on (d). (d) Study sites and measurement locations. Green crosses are the locations of targets used for LiDAR georeferencing. Small purple dots are the locations of the drilling measurements performed on 27 May 2015. Larger purple dots are the stake locations. The blue dashed line is the ski way. The orange star is the location of the automatic weather station (AWS). The thick black line delimits the entire area scanned with the terrestrial LiDAR. The dashed black line shows the boundary of the interpolations made in the study.
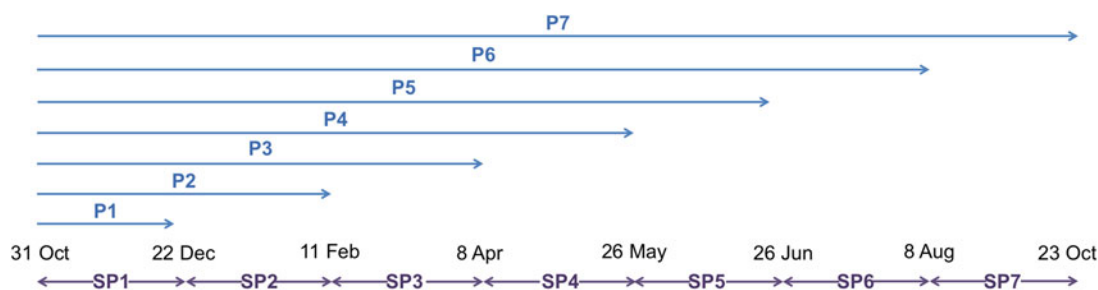

Fig. 2. Definition of periods (Pi) and sub-periods (SPi) over the year of measurements.

Table 1. Summary of measurements performed during each field campaign over the entire year

Date	LiDAR	Surface mass balance (from 31 October) using drilling cores	Density	Surface mass balance at each of the 5 stakes	5 stake positions (DGPS)	Weather Station
31/10/2014	Yes	Reference	–	–	–	–
22/12/2014	Yes	No	One measurement down to 1.4 m	–	–	–
11/02/2015	Yes	5 measurements: at each stake	One at stake #4	Stakes set up	Stakes set up	AWS installed
09/03/2015	No	No	No	Yes	No	Data downloaded
08/04/2015	Yes	1 measurement at stake #4	One at stake #4	Yes	Yes	Station raised
27/05/2015	Yes	15 measurements over the entire area	2 measurements: at drilling site #6 and stake #2	Yes	Yes + inclination	Data downloaded
26/06/2015	Yes	1 measurement at stake #2	One at stake #2	Yes	Yes	Data downloaded
08/08/2015	Yes	1 measurement at stake #4	One at stake #4	Yes	Yes	Data downloaded
23/10/2015	Yes	1 measurement at stake #4	One at stake #4	Yes	Yes	Station dismantled

merged. Then, for the georeferencing of the merged point cloud resulting from each survey, the 3D coordinates of six targets were measured using a differential GPS (D-GPS). For this, we used a Leica 1200 Differential Global Positioning System (GNSS) receiver, running with dual frequencies. Occupation times were typically 1 min with one second sampling and the number of visible satellites (GPS and GLONASS) was >7. The distance between fixed and mobile receivers was less than a kilometer. The DGPS positions have an intrinsic accuracy of ±0.01 m. Considering this DGPS uncertainty and the manual measurement uncertainty when measuring the target center, we consider the accuracy to be ±0.03 m. Finally, the georeferenced point clouds were rasterized using the nearest neighbor method to obtain eight 1 m resolution DEMs with a horizontal and vertical uncertainty related to the alignment and the georeferencing of 3 and 10 cm, respectively.

3.2 Surface mass-balance measurements

3.2.1 Drilling cores
Several snow-accumulation measurements using a PICO three-inch (7.62 cm) hand ice-coring system were performed during each of the eight field campaigns, drilling cores down to the end-of-summer layer, easily identifiable from changes in snow grain size and the dust deposited during the previous summer

period. This method quantifies the total surface mass balance since the beginning of the winter season (i.e., October 2014). Note that the October surface (or end-of-summer) is considered as the reference layer before the accumulation and matches the surface measured with the LiDAR in October 2014 as almost no precipitation occurred during the month of October 2014 (3.5 mm w.e. accumulated over the month), i.e., before the LiDAR scan on 31 October 2014. Furthermore, snow profile measurements made in the first meter of the snowpack at this time showed grain size and type corresponding to metamorphosed snow, supporting the interpretation that the 31 October surface was the snow layer representative of the end-of-summer surface.

For each campaign, one core was drilled close to the AWS, providing the snow depth and density (more details in Table 1). During the campaign on 27 May 2015, roughly at the end of the accumulation season, 15 cores (see locations in Fig. 1), including two density measurements, were drilled over the accessible parts of the study area.

3.2.2 Stakes

Five 5 m long wooden poles with a diameter of 12 cm were inserted to a depth of 1 m on 11 February 2015. These five stakes were distributed over the central part of the study area (Fig. 1c). Locations were chosen according to accessibility, without disturbing the ski way, which is very busy with tourism during wintertime. During each field campaign, the snow depth changes were measured by calculating the differences in stake emergence (i.e., following the glaciological method, more details in Table 1) with an estimated accuracy of ±0.05 m (uncertainty mainly related to the slight tilt of the stakes).

3.3 Submergence velocity

As defined by Cuffey and Paterson (2010), the emergence velocity corresponds to the upward or downward displacement relative to the glacier surface, which can be defined at a fixed coordinate or for a coordinate that moves with the flow. In the accumulation area, it is called the submergence velocity and is due to the ice motion and snow/firn densification. It corresponds to the downward vertical displacement corrected for slope and is defined by Eqn (1).

$$w_{sub} = w_s - u_s \frac{dZs}{dx} - v_s \frac{dZs}{dy}, \qquad (1)$$

where u_s, v_s, w_s are the components of the velocity vector of the glacier flow, Z_s is the elevation of the glacier surface and x, y the coordinates. At a given point, the glacier surface elevation changes according to the sum of submergence velocities and the amount of mass (i.e., snow, ice) added to the surface. Note that submergence velocity differs from the velocity of the vertical displacement of the stakes (which is defined by the vertical changes at rate w_s). In this study, two in situ methods were used to measure the submergence velocity and are described below.

3.3.1 Method 1: measurements at each core drilling site

This method ($M1$) is an Eulerian approach that calculates the submergence velocity for fixed points, independent of time. For this purpose, the elevation of the end-of-summer layer ($Zs_{EndSummer\_Oct}$, in m a.s.l.) was measured during the first LiDAR acquisition performed on 31 October 2014, with an uncertainty estimated at ±0.10 m (see Section 3.1). The elevation of the same layer was then measured again in May 2015

($Zs_{EndSummer\_May}$, in m a.s.l.) for each of the 15 core drilling sites using the height of the snow mantle from drilling cores (with an uncertainty of ±0.20 m, Thibert and others, 2008) and D-GPS measurements (with an uncertainty of ±0.03 m). The elevation difference between the two dates represents the submergence velocity. Therefore, based on these measurements, the submergence velocity at each point (w_{sub}) can be computed using Eqn (2), with an uncertainty of $\sim \pm 0.22$ m, quantified from the propagation of errors, considering uncertainties related to LiDAR, drilling cores and DGPS measurements.

$$w_{sub}(M1) = \frac{Zs_{EndSummer\_May} - Zs_{EndSummer\_Oct}}{Time}. \qquad (2)$$

3.3.2 Method 2: measurement using stakes

The second method ($M2$) is a Lagrangian approach that follows the location of a point and is time dependent. This method involves measuring the locations of the tops of the five stakes. These locations were accurately measured using a D-GPS during each campaign, from 11 February 2015 onward, to quantify vertical and horizontal location changes of the stakes. For each measurement, the slope of the surface (α) is calculated over the distance of the horizontal displacement of the stake between two campaigns. The slope is computed from the LiDAR-derived DEM measured at each campaign. This slope is considered to quantify the submergence velocities using this method (Eqn. 3). Uncertainties of this method are related to: (i) D-GPS measurements (±0.03 m corresponding to the DGPS accuracy (see Section 3.1) and the size of the holes drilled to insert the stakes), (ii) the slope estimation (±0.04 m, corresponding to a slope difference of 1°), and (iii) the stake inclination over time due to glacier flow (±0.03 m). Considering all these uncertainties, the submergence-velocity uncertainty for the period from February to May is computed using the propagation error approach and is equal to ±0.18 m ($\sim \pm 0.50$ m per year) using this method.

$$w_{sub}(M2) = w_s - u_s \tan\alpha . \qquad (3)$$

3.4 Surface mass-balance maps

Surface mass-balance maps were plotted using the differences between the DEMs acquired with the LiDAR measurements and correcting these DEM differences using the submergence velocities. For this, the submergence velocities quantified at a point scale have been interpolated using a Kriging method. Interpolation uncertainty is computed using a leave-one-out cross-validation method, i.e., performing repeated interpolations based on 14 of the 15 points, keeping one point for uncertainty estimation. Finally, surface mass-balance maps are compared to local measurements to evaluate the method uncertainty.

3.5 Automatic weather station measurements

An AWS was set up on 11 February 2014 at Col du Midi (see location on Fig. 1) and recorded meteorological measurements continuously (without a data gap) until 23 October 2015 (Table 1). The air temperature, relative humidity (measured with a VAISALA HMP155 sensor), wind speed and direction (measured with an RM Young 05103 sensor) and snow depth (using an SR50 Campbell sonic ranger) were recorded at an hourly time step. These data were used to interpret the variability of the surface mass balance as discussed in Section 5. Daily precipitation from SAFRAN reanalysis data (Durand and others, 2009) was
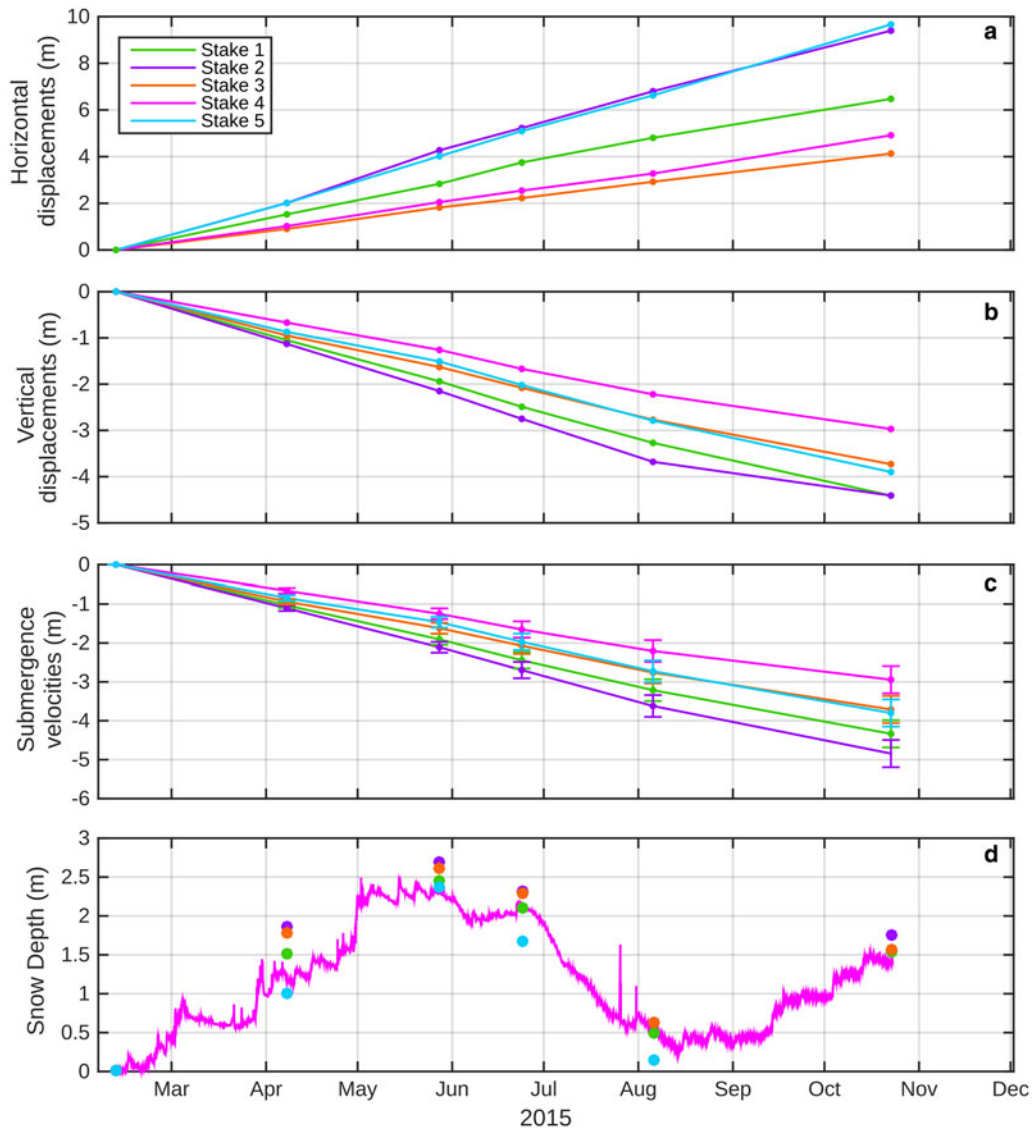
Fig. 3. (a) Horizontal displacements and (b) vertical displacements, and (c) submergence velocities, measured at each stake over the period 11 February 2015–23 October 2015. (d) The pink line is the snow depth measured at the automatic weather station (i.e., Stake 4) and the dots represent the snow depth measured at each stake.

also used. SAFRAN disaggregates large-scale meteorological analyses and observations in the French Alps. The analyses provide hourly meteorological data for seven slope exposures (N, S, E, W, SE, SW and flat) and altitudes at 300 m intervals up to 3600 m a.s.l.

4. Results

4.1 Horizontal velocities

Figure 3a shows the horizontal displacements of the five stakes over the period 11 February to 23 October 2015. The almost linear evolution of the horizontal displacements indicates constant velocities throughout the measurement period. Surface velocities measured at the five stakes are 9.3, 13.5, 5.9, 7.1 and 13.9 $\pm$ 0.2 m a^{-1} for stakes 1–5, respectively. The differences in horizontal displacement from site to site indicate high spatial variability. For instance, the difference between stake 3 and 5, <400 m apart, is 5.6 m (for the period between 11 February and 23 October), corresponding to 8 m a^{-1}. Despite the low horizontal surface velocities (<14 m a^{-1}), the fastest velocities are observed at the steepest locations (i.e., at stake 5 with a slope of ∼3°).

4.2 Submergence velocities

4.2.1. Quantification using stakes

Vertical displacements measured at each stake for the period between 11 February and 23 October 2015 and vertical displacements corrected for slope are reported in Figures 3b, c. Similar to the horizontal displacements, results show an almost linear temporal evolution at each stake, indicating constant submergence velocities throughout the measurement period. The temporal changes are lower than the measurement uncertainty and do not reveal significant seasonal changes. The submergence velocity can be extrapolated over the total study period (31 October 2014–23 October 2015).

Figure 3b also indicates a strong spatial variability of the vertical displacements. The largest difference is observed between stakes 2 and 4, with a difference of 2.7 m a^{-1}, which is a factor of 1.6 between these two stakes. Because of the high spatial variability, a dense and distributed measurement network over the entire study area would be required to establish the most accurate submergence-velocity map possible, which could be used to correct the LiDAR DEMs differences from the submergence velocity. As stakes cover only a small part of the scanning area (Fig. 1), the
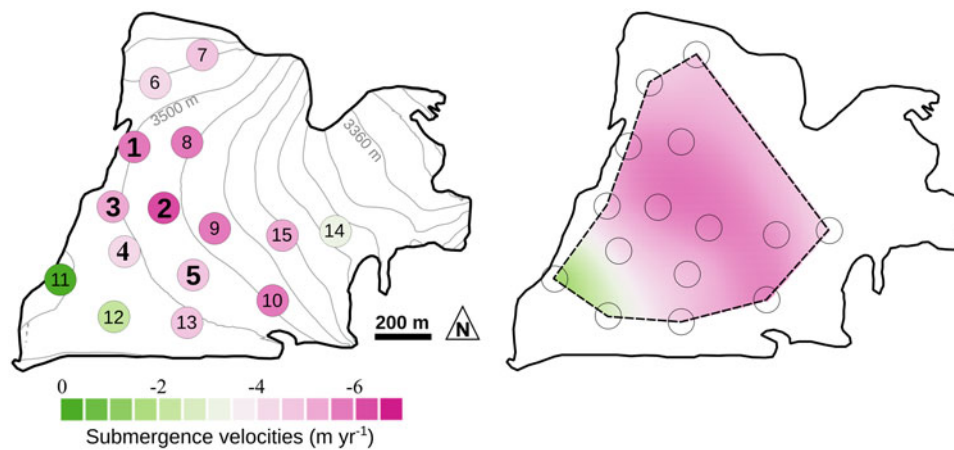
Fig. 4. (Left): Submergence velocities at each drilling site computed using method 1 (method detailed in Section 3.3.1). Cores drilled close to the stakes are indicated in bold by the corresponding stake numbers. (Right): Interpolation of the submergence velocities with a Kriging method.

submergence measurements at the stakes are supplemented by the measurements from the 15 core drilling sites.

4.2.2 Using drilling cores

Figure 4 represents the submergence velocities computed using method 1 based on an Eulerian approach ($w_{sub}(M1)$) and shows strong spatial variability (ranging from 2.1 to 5.9 m a^{-1}). The average distance between two measurements is ~250 m, for an average difference of submergence velocity of 0.68 m a^{-1}. This difference can be larger than 1 m a^{-1} for two measurement sites 300 m apart (e.g., cores #4 and #12 in Fig. 4).

4.2.3 Comparison of results of the two methods

The correlation between the submergence velocities obtained with the two methods ($w_{sub}(M1)$ and $w_{sub}(M2)$ described in Section 3.3) is significant ($r^2 = 0.93$) with a confidence level of 99% according to the Student's t-test. As $w_{sub}(M1)$ is computed using measurements over the period October 2014–May 2015 and $w_{sub}(M2)$ over the total period February–October 2015, the values were extrapolated over 1 year to allow comparison. Differences range between 0.06 m a^{-1} (stake #1) and 0.31 m a^{-1} (stake #4), without systematic bias, and the RMSE equals 0.23 m a^{-1}, which is lower than the measurement uncertainty.

In addition, the spatial variability of the submergence velocities agrees well for the two approaches even if only five point comparisons are available. For instance, whatever the method used, the largest difference between the quantified submergence velocities is observed for stakes #2 and #4; this spatial difference equals 2.3 and 2.7 m a^{-1} for $w_{sub}(M1)$ and $w_{sub}(M2)$, respectively.

4.2.4 Submergence-velocity map and uncertainty

Because of (i) the good agreement between the two methods used to quantify the submergence velocities, (ii) the linear temporal evolution of the submergence velocities, and (iii) the need for an accurate representation of the spatial distribution of the submergence velocities, the submergence velocities were interpolated using a Kriging method. Interpolation uncertainty is evaluated using a leave-one-out cross-validation method, i.e., performing repeated interpolations based on 14 of the 15 points, keeping one point for uncertainty estimation. When the point used for the interpolation uncertainty estimate is located within the area defined by the measurement network, the average difference between the measured and interpolated value is 0.13 m a^{-1} with a maximum of 0.23 m a^{-1}. On the other hand, when the point is located on the edge of the study area, the difference can reach values of more than 1 m a^{-1}. According to these results,

the surface mass-balance maps (Section 4.3) are restricted to the area defined within the measurement network. The uncertainty related to the interpolation method on submergence velocities is assumed to be equal to ±0.13 m a^{-1}.

4.3 Surface mass-balance maps

Figure 5 shows the surface mass-balance maps (SMB$_{LiDAR}$) since 31 October 2014. These results were obtained using the difference between the successive DEMs acquired by the LiDAR measurements (described in Section 3.1), while also correcting the DEM difference for the glacier dynamics using the submergence-velocity map (described in Section 4.1.4). To validate the method and evaluate the uncertainties, the SMB$_{LiDAR}$ maps are compared with the 25 local in situ surface mass-balance measurements performed at each stake (SMB$_m$, indicated by the circles in Fig. 5). Results indicate a very good agreement ($r^2 = 0.92$, $p < 0.05$, RMSE = 0.27 m) with a maximum difference of 0.49 m.

Note that the measurements performed in May are not used in this comparison (Fig. 5e) given that they have been used to quantify the submergence velocity map. In addition, the absence of surface mass-balance measurements using the drilling method in December prevents validation over the period October 2014–December 2014 (Fig. 5b).

The uncertainty in the SMB$_{LiDAR}$ is estimated by computing the quadratic sum of the uncertainty due to LiDAR measurements (±0.20 m) related to the DEM acquisitions, the uncertainty related to the calculation of the submergence velocities (±0.50 m a^{-1}) and the uncertainty linked to the interpolation of the submergence velocities (±0.13 m a^{-1}). This uncertainty ranges from ±0.36 m (for the period October to February) to ±0.55 m (for the entire period: October 2014 to October 2015).

Results presented in Figure 5 show a significant spatial variability of the surface mass balance. Indeed, the std dev. of the surface mass-balance maps for each period are 0.28, 0.52, 0.92, 0.79, 0.78, 0.73 and 0.78 m for P1 to P7, respectively.

5. Discussion

5.1 Submergence velocities and surface mass balance

At steady state, the surface mass balance can be directly estimated from the submergence velocity (Eqn. 1; Cuffey and Paterson, 2010). The annual surface mass balance measured at the five stakes in October 2015 was compared to the submergence velocities. Note that the density profile measured by drilling in October
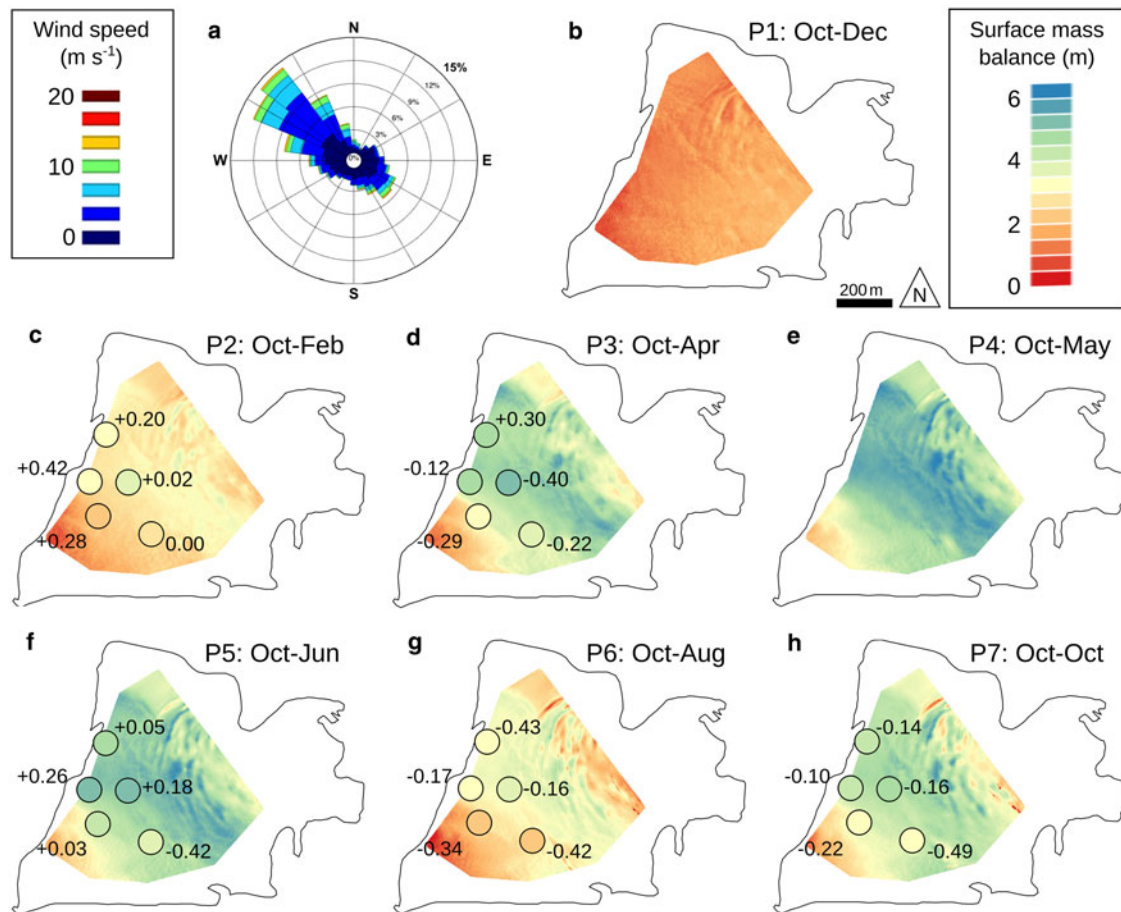
Fig. 5. (a) Wind rose from the half-hourly mean measurements at the weather station over the period February – October 2015. (b) to (h) Surface mass-balance maps (SMB$_{LiDAR}$) for each period, Pi, with $i \, \varepsilon$ [1; 7], i.e., since October 2014. Colored circles indicate winter surface mass balances measured at the same date with the drilling method (SMB$_m$). Numbers indicated close to the circle correspond to the differences in meters between SMB$_m$ and SMB$_{LiDAR}$, positive differences meaning SMB$_m$ > SMB$_{LiDAR}$.

2015 was used to convert the annual surface mass balance and submergence velocities into water equivalent (w.e.). As the density was measured at only one site, we assume a homogeneous density over the whole area. Despite this questionable assumption on the density, the comparison between the submergence velocities and the annual surface mass balance (Fig. 6) indicates an excellent correlation. The bias of 1.23 m w.e. a^{-1} indicates a non-steady state in this part of the glacier. It confirms the surface elevation lowering shown from the DEMs difference (Fig. S3 in the Supplementary material).

In addition, our comparison shows a very good agreement between the spatial variability of the submergence velocity and the surface mass balance with an RMSE of 0.08 m w.e. These differences are within the uncertainties. Note that the submergence velocities appear to offer a good way of assessing the long-term average surface mass balance (Vincent and others, 2007b). From our comparison, we can conclude that the annual mass balances correlate very well with submergence velocities.

5.2 Spatio-temporal variability of the surface mass balance

Our results clearly show a strong spatio-temporal variability of the surface mass-balance distribution, mainly during the winter period (Fig. 5). The relationships with topographical parameters have been reported in some studies to be significant (e.g., Sold and others, 2015). In our case, wind effects are expected to be the main driver for the spatial variability because (i) the elevation range of the study area is limited (i.e., <250 m, with a std dev. equal to 25 m) and therefore no precipitation gradient is expected and (ii) slopes are low (i.e., 2° on the average and always <11°) meaning that avalanches are not observed at that site. This assumption is reinforced by the finding of a previous study performed by Réveillet and others (2017) over the accumulation zone of the Mer de Glace. Based on the accumulation measurements conducted each year with the glaciological method over the period 1995–2014, they failed to find significant relationships between winter surface mass-balance spatial variability and the classical topographic variables found in the literature (i.e., elevation, curvature, distance to steep slope and ridge and topographic position index). Nevertheless, this study was performed using only a few stakes (seven in the accumulation part of the glacier and only two overlapping with the area of the current study) and one of the conclusions was the need to quantify the spatio-temporal variability at a higher resolution to be able to better understand this variability and to relate it to indexes considering wind effects.

The significant impact of wind effect on the snow distribution has been reported in several studies over mountain regions and glaciers using the Sx index (e.g., Winstral and others, 2002, Erickson and others, 2005; McGrath and others, 2015; Molotch and others, 2005; Grunewald and others, 2013, Revuelto and others, 2014). Some studies indicated that this variable was the main contributor to spatial variability, sometimes even more than elevation (e.g., Grünewald and others, 2013). Therefore, it has been advised to take this index into account in model studies (Grünewald and others, 2013). In our case, the surface mass-
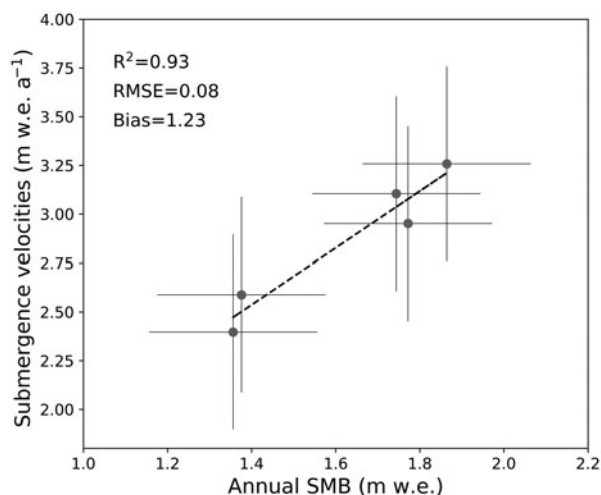
Fig. 6. Correlation between the annual surface mass balance (SMB) and the submergence velocity. Error bars represent measurement uncertainties.

balance maps presented in this study (Fig. 5) were compared to the Sx index computed for each gridcell for each period and sub-period (see Supplementary material for the complete description). Despite its importance in explaining the snow-accumulation distribution as reported by Winstral and Marks (2014) and Revuelto and others (2014), our results indicate a highly variable correlation from one period to another depending on specific wind conditions during and after the snowfalls. In addition, the best correlation is obtained for wind directions that often do not match the main measured wind direction. On the other hand, note that the highest correlations are found at the beginning of the accumulation season (S2 in the Supplementary material) and can be related to snow layers with a lower density (e.g., 0.2 measured for the first 50 cm of the snowpack in February), thus more erodible and transportable by wind; compared with the end of the season when higher temperature and snow depth can lead to a denser snow pack (e.g., 0.4 measured for the first 50 cm in May) that is therefore less subject to erosion and transportation.

Note that our dataset might not be fully suited to the use of the Sx index. Indeed, our maps are quantified at roughly a monthly scale and therefore integrate a large variety of snowfall events (with different amounts, influenced by different wind directions during and after each event). For instance, observations from the AWS show several changes of wind direction over a short time period (e.g., the event in March had a WNW direction during the snowfall and changed to S just after the snowfall) associated with erosion processes (Fig. 3d and Fig. S1 in the Supplementary material). Therefore, in our context, it is difficult to draw conclusions on the relationship between the spatial variability of surface mass balance over a period of about a month and the Sx index. We therefore suggest that this index should be used at the snowfall event scale.

5.3 Limitations of the study and further work

Despite the 2 km^2 scanned area, our study covers only a limited portion of the accumulation area of the Mer de Glace and represents <10% of the total area of the glacier (28 km^2). This study merits extension to a larger scale. However, given the amount of fieldwork required in this study, extension to a wider spatial scale would be extremely difficult. Additional measurements from other techniques such as the acquisition of DEM from airborne LiDAR, high-resolution remote sensing (e.g., Pléiades or drone) or GPR measurements (even if it is limited to accessible

areas) would be required. In such a context, combined approaches would enable uncertainties to be quantified as has been done in other studies based on LiDAR measurements (e.g., Carturan and others, 2013; Sold and others, 2013; Piermattei and others, 2015, 2016; Fischer and others, 2016).

Nevertheless, whatever the chosen method, it is necessary to properly consider the submergence velocities. The strong spatial variability of the submergence velocity confirms the need for a dense measurement network to accurately correct the DEM differences for glacier dynamics and obtain the surface mass-balance map at the glacier surface. For further studies, we recommend prioritizing their measurement over a large area. This could be done, for instance, using GPR measurements that can cover a larger area with a higher spatial resolution (e.g., Sold and others, 2013; Schöber and others, 2014). Note that the geodetic mass-balance method does not require submergence/emergence velocity corrections given that the DEM difference provides the mass change of the entire glacier.

Finally, an accurate quantification of the submergence velocities provides valuable and useful information to calibrate or validate physical ice-flow models, which is essential to simulate future glacier evolution.

6. Conclusion

The main aim of this study was to evaluate the spatial distribution of surface mass balance in the accumulation zone of the Mer de Glace over the 2014–2015 hydrological year using monthly terrestrial LiDAR acquisitions. For this, the difference between DEMs obtained by LiDAR scans needs to be corrected to account for the submergence velocities. The in situ measured submergence velocities indicate a linear temporal evolution of both vertical and horizontal displacements, without significant seasonal changes over the study period (i.e., from February to October 2015). On the other hand, these measurements show a significant spatial variability (with a mean of 4.5 m a^{-1}, a std dev. of 1.5 m a^{-1} and a maximum difference reaching 5.9 m a^{-1}), demonstrating the importance of a dense network of submergence-velocity measurements to reduce the uncertainties when correcting the DEM differences to compute the surface mass balance.

Our results also indicate a high spatio-temporal variability of the surface mass-balance distribution even if at first glance the topography of the study area is relatively homogeneous. In this area, located close to a pass, wind seems to be one of the main causes of the spatial variability at decametric-to-hectometric scales. Nevertheless, correlations between the Sx index and surface mass balance over the winter period are poor and the highest correlations are not found with the main measured wind direction. This points out the limitation in using this index for long time periods, rather than at the event scale, given that the snow spatial distribution, for instance on a monthly scale, can be related to distinct wind directions.

For further studies, given the significant spatial variability of the submergence velocities, we recommend prioritizing their measurement over a large area. This could be done, for instance, using radar measurements that can cover a wider area with a higher spatial resolution.

References

Baltsavias EP (1999) A comparison between photogrammetry and laser scanning. *ISPRS Journal of Photogrammetry and Remote Sensing* **54**, 83–94.

Braithwaite RJ and Zhang Y (2000) Sensitivity of mass balance of five Swiss glaciers to temperature changes assessed by tuning a degree-day model. *Journal of Glaciology* **46**(152), 7–14.

Bruland O, Liston GE, Vonk J, Sand K and Killingtveit A (2004) Modelling the snow distribution at two high Arctic sites at Svalbard, Norway, and at an alpine site in central Norway. *Hydrology Research* **35**, 191–208.

Bühler Y, Adams MS, Bösch R and Stoffel A (2016) Mapping snow depth in alpine terrain with unmanned aerial systems (UASs): potential and limitations. *The Cryosphere* **10**, 1075–1088. doi: 10.5194/tc-10-1075-2016

Carturan L and 11 others (2013) Current behaviour and dynamics of the lowermost Italian glacier (montasio occidentale, julian alps). *Geografiska Annaler: Series A, Physical Geography* **95**(1), 79–96. doi: 10.1111/geoa.12002

Cogley JG and 10 others (2011) Glossary of Glacier Mass Balance and Related Terms, *IHP-VII Technical Documents in Hydrology* No. 86, IACS Contribution No. 2, UNESCO-IHP, Paris.

Cuffey KM and Paterson WSB (2010) *The Physics of Glaciers*, 4th edition, Oxford: Academic Press, Butterworth-Heinemann.

Dadic R, Mott R, Lehning M and Burlando P (2010) Wind influence on snow depth distribution and accumulation over glaciers. *Journal of Geophysical Research Earth Surfaces* **115**, F01012. doi: 10.1029/2009JF001261.

Davaze L, Rabatel A, Dufour A, Arnaud Y and Hugonnet R (2020) Region-wide annual glacier surface mass balance for the European Alps from 2000 to 2016. *Frontiers in Earth Science* **8**, 149.

Deems JS, Painter TH and Finnegan DC (2013) Lidar measurement of snow depth: a review. *Journal of Glaciology* **59**(215), 467–479. doi: 10.3189/2013JoG12J154

Dunse T and 5 others (2009) Recent fluctuations in the extent of the firn area of Austfonna, Svalbard, inferred from GPR. *Annals of Glaciology* **50**, 155–162. doi: 10.3189/172756409787769780

Durand Y and 5 others (2009) Reanalysis of 44 Yr of climate in the French Alps (1958–2002): methodology, model validation, climatology, and trends for air temperature and precipitation. *Journal of Applied Meteorology and Climatology* **48**, 429–449. doi: 10.1175/2008JAMC1808.1

Erickson TA, Williams MW and Winstral A (2005) Persistence of topographic controls on the spatial distribution of snow in rugged mountain terrain, Colorado, United States. *Water Resources Research* **41**(4), W04014. doi: 10.1029/2003WR002973

Fassnacht S and Deems J (2006) Measurement sampling and scaling for deep montane snow depth data. *Hydrological Processes* **20**, 829–838. doi: 10.1002/hyp.6119

Fischer M, Huss M, Kummert M and Hoelzle M (2016) Application and validation of long-range terrestrial laser scanning to monitor the mass balance of very small glaciers in the Swiss Alps. *The Cryosphere* **10**(3), 1279–1295. doi: 10.5194/tc-10-1279-2016

Gabbi J, Carenzo M, Pellicciotti F, Bauder A and Funk M (2014) A comparison of empirical and physically based glacier surface melt models for long-term simulations of glacier response. *Journal of Glaciology* **60**(224), 1140–1154. doi: 10.3189/2014JoG14J011

Gabbud C, Micheletti N and Lane SN (2015) Lidar measurement of surface melt for a temperate Alpine glacier at the seasonal and hourly scales. *Journal of Glaciology* **61**(229), 963–974. doi: 10.3189/2015JoG14J226

Gaillardet J and others (2018) OZCAR: the French network of critical zone observatories. *Vadose Zone Journal* **17**(1), 80067. doi: 10.2136/vzj2018.04.0067.

Gerbaux M, Genthon C, Etchevers P, Vincent C and Dedieu JP (2005) Surface mass balance of glaciers in the French Alps: distributed modelling and sensitivity to climate change. *Journal of Glaciology* **51**(175), 561–572. doi: 10.3189/172756505781829133

Grünewald T and 9 others (2013) Statistical modelling of the snow depth distribution in open alpine terrain. *Hydrology and Earth System Science* **17**, 3005–3021. doi: 10.5194/hess-17-3005-2013

Grünewald T and Lehning M (2011) Altitudinal dependency of snow amounts in two small alpine catchments: can catchment-wide snow amounts be estimated via single snow or precipitation stations? *Annals of Glaciology* **52**(58), 153–158. doi: 10.3189/172756411797252248

Grünewald T, Schirmer M, Mott R and Lehning M (2010) Spatial and temporal variability of snow depth and ablation rates in a small mountain catchment. *The Cryosphere* **4**, 215–225. doi: 10.5194/tc-4-215-2010

Haeberli W and Beniston M (1998) Climate change and its impacts on glaciers and permafrost in the Alps. *Ambio* **27**(4), 258–265.

Heilig A, Eisen O and Schneebeli M (2010) Temporal observations of a seasonal snowpack using upward-looking GPR. *Hydrological Processes* **24**, 3133–3145. doi: 10.1002/hyp.7749

Helfricht K and 5 others (2012) Snow accumulation of a high alpine catchment derived from LiDAR measurements. *Advances in Geosciences* **32**, 31–39. doi: 10.5194/adgeo-32-31-2012

Hock R (1999) A distributed temperature-index ice-and snowmelt model including potential direct solar radiation. *Journal of Glaciology* **45**(149), 101–111. doi: 10.3189/S0022143000003087

Huss M and Bauder A (2009) 20th-century climate change inferred from four long-term point observations of seasonal mass balance. *Annals of Glaciology* **50**(50), 207–214. doi: 10.3189/172756409787769645

Kääb A and Funk M (1999) Modelling mass balance using photogrammetric and geophysical data: a pilot study at Griesgletscher, Swiss Alps. *Journal of Glaciology* **45**(151), 575–583.

Kirchner P, Bales R, Molotch N, Flanagan J and Guo Q (2014) LiDAR measurement of seasonal snow accumulation along an elevation gradient in the southern Sierra Nevada, California. *Hydrology and Earth System Science* **18**, 4261–4275. doi: 10.5194/hess-18-4261-2014

Kühn M (2003) Redistribution of snow and glacier mass balance from a hydrometeorological model. *Journal of Hydrology* **282**(1–4), 95–103. doi: 10.1016/S0022-1694(03)00256-7

Liston GE and Sturm M (1998) A snow-transport model for complex terrain. *Journal of Glaciology* **44**(148), 498–516.

López-Moreno JI, Fassnacht S, Beguería S and Latron J (2011) Variability of snow depth at the plot scale: implications for mean depth estimation and sampling strategies. *The Cryosphere* **5**, 617–629. doi: 10.5194/tc-5-617-2011

López-Moreno JI and Stähli M (2008) Statistical analysis of the snow cover variability in a subalpine watershed: assessing the role of topography and forest interactions. *Journal of Hydrology* **348**, 379–394. doi: 10.1016/j.jhydrol.2007.10.018

Lutz E, Geist T and Stötter J (2003) Investigations of airborne laser scanning signal intensity on glacial surfaces – utilising comprehensive laser geometry modelling and orthophoto surface modelling (a case study: Svartisheibreen, Norway). *International Archives of Photogrammetry, Remote Sensing and Spatial Information Science* **34**(3W13), 143–148.

Machguth H, Eisen O, Paul F and Hoelzle M (2006) Strong spatial variability of snow accumulation observed with helicopter-borne GPR on two adjacent Alpine glaciers. *Geophysical Research Letters* **33**, L13503. doi: 10.1029/2006GL026576.

Machguth H, Paul F, Kotlarski S and Hoelzle M (2009) Calculating distributed glacier mass balance for the Swiss Alps from regional climate model output: a methodical description and interpretation of the results. *Journal of Geophysical Research* **114**, D19106. doi: https://doi.org/10.1029/2009JD011775.

Marti R and 5 others (2016) Mapping snow depth in open alpine terrain from stereo satellite imagery. *The Cryosphere* **10**, 1361. doi: 10.5194/tc-10-1361-2016

McGrath D and 7 others (2015) End-of-winter snow depth variability on glaciers in Alaska, *Journal of Geophysical Research in Earth Surface* **120**, 1530–1550. doi: 10.1002/2015JF003539

Molotch NP, Colee MT, Bales RC and Dozier J (2005) Estimating the spatial distribution of snow water equivalent in an alpine basin using binary regression tree models: the impact of digital elevation data and independent variable selection. *Hydrological Processes* **19**(7), 1459–1479. doi: 10.1002/hyp.5586

Oerlemans J and Reichert BK (2000) Relating glacier mass balance to meteorological data by using a seasonal sensitivity characteristic. *Journal of Glaciology* **46**(152), 1–6.

Paul F, Kääb A, Maisch M, Kellenberger T and Haeberli W (2004) Rapid disintegration of Alpine glaciers observed with satellite data. *Geophysical Research Letters* **31**(21), L21402. doi: 10.1029/2004GL020816

Pellicciotti F and 5 others (2005) An enhanced temperature-index glacier melt model including the shortwave radiation balance: development and wtesting for Haut Glacier d'Arolla, Switzerland. *Journal of Glaciology* **51**(175), 573–587. doi: 10.3189/172756505781829124

Piermattei L and 6 others (2016) Suitability of ground-based SfM-MVS for monitoring glacial and periglacial processes. *Earth Surface Dynamics* **4**(2), 425–443. doi: 10.5194/esurf-4-425-2016

Piermattei L, Carturan L and Guarnieri A (2015) Use of terrestrial photogrammetry based on structure-from-motion for mass balance estimation of a small glacier in the Italian Alps. *Earth Surface Processes and Landforms* **40**(13), 1791–1802. doi: 10.1002/esp.3756

Prokop A (2008) Assessing the applicability of terrestrial laser scanning for spatial snow depth measurements. *Cold Regions Science and Technology* **54**, 155–163.

Pulwicki A, Flowers GE, Radić V and Bingham D (2018) Estimating winter balance and its uncertainty from direct measurements of snow depth and density on alpine glaciers. *Journal of Glaciology* **64**(247), 781–795. doi: 10.1017/jog.2018.68

Rabatel A, Dedieu JP, Thibert E, Letréguilly A and Vincent C (2008) 25 Years (1981–2005) of equilibrium-line altitude and mass-balance reconstruction on Glacier Blanc, French Alps, using remote-sensing methods and meteorological data. *Journal of Glaciology* **54**(185), 307–314. doi: 10.3189/002214308784886063

Réveillet M and 7 others (2018) Relative performance of empirical and physical models in assessing the seasonal and annual glacier surface mass balance of Saint-Sorlin Glacier (French Alps). *The Cryosphere* **12**(4), 1367–1386. doi: 10.5194/tc-12-1367-2018.

Réveillet M, Vincent C, Six D and Rabatel A (2017) Which empirical model is best suited to simulate glacier mass balances? *Journal of Glaciology* **63**(237), 39–54. doi: 10.1017/jog.2016.110

Revuelto J, López-Moreno JI, Azorin-Molina C and Vicente-Serrano SM (2014) Topographic control of snowpack distribution in a small catchment in the central Spanish Pyrenees: intra- and inter-annual persistence. *The Cryosphere* **8**, 1989–2006. doi: 10.5194/tc-8-1989-2014

Rohrer M, Braun L and Lang H (1994) Long-term records of snow cover water equivalent in the Swiss Alps. *Hydrology Research* **25**, 53–64.

Schöber J and 6 others (2014) Snow cover characteristics in a glacierized catchment in the Tyrolean Alps-improved spatially distributed modelling by usage of Lidar data. *Journal of Hydrology* **519**, 3492–3510.

Six D and Vincent C (2014) Sensitivity of mass balance and equilibrium-line altitude to climate change in the French Alps. *Journal of Glaciology* **60**, 867–878. doi: 10.3189/2014JoG14J014

Sold L and 5 others (2013) Methodological approaches to infer end-of-winter snow distribution on alpine glaciers. *Journal of Glaciology* **59**, 1047–1059. doi: 10.3189/2013JoG13J015

Sold L, Huss M, Eichler A, Schwikowski M and Hoelzle M (2015) Unlocking annual firn layer water equivalents from ground-penetrating radar data on an Alpine glacier. *The Cryosphere* **9**, 1075–1087. doi: 10.5194/tc-9-1075-2015

Solomon S, Manning M, Marquis M and Qin D (2007) *Climate Change 2007-the Physical Science Basis: Working Group I Contribution to the Fourth Assessment Report of the IPCC*, vol. **4**. Cambridge, UK: Cambridge University Press.

Thibert E, Blanc R, Vincent C and Eckert N (2008) Instruments and methods; glaciological and volumetric mass-balance measurements: error analysis over 51 years for Glacier de Sarennes, French Alps. *Journal of Glaciology* **54**(186), 522–532. doi: 10.3189/002214308785837093

Trujillo E and Lehning M (2015) Theoretical analysis of errors when estimating snow distribution through point measurements. *The Cryosphere* **9**, 1249–1264. doi: 10.5194/tc-9-1249-2015

Trujillo E, Ramírez JA and Elder KJ (2007) Topographic, meteorologic, and canopy controls on the scaling characteristics of the spatial distribution of snow depth fields. *Water Resources Research* **43**, W07409. doi: 10.1029/2006WR005317.

Vincent C (2002) Influence of climate change over the 20th century on four French glacier mass balances. *Journal of Geophysical Research* **107**(D19), 4375. doi: 10.1029/2001JD000832.

Vincent C and 5 others (2007a) Climate warming revealed by englacial temperatures at Col du Dôme (4250 m, Mont Blanc area): englacial temperature (Mt Blanc Area). *Geophysical Research Letters* **34**, L16502. doi: 10.1029/2007GL029933.

Vincent C and 5 others (2007b) Very hight elevation Mont-Blanc glaciated areas not affected by the 20th century climate change. *Journal of Geophysical Research: Atmospheres* **112**, D09120. doi: 10.1029/2006JD007407

Vincent C, Vallon M, Pinglot J, Reynaud L and Funk M (1997) Snow accumulation and ice flow at Dôme du Goûter (4300 m), Mont Blanc, French Alps. *Journal of Glaciology* **43**, 513–521.

Wehr A and Lohr U (1999) Airborne laser scanning an introduction and overview. *ISPRS Journal of Photogrammetry and Remote Sensing* **54**, 68–82.

Winstral A and Marks D (2002) Simulating wind fields and snow redistribution using terrain-based parameters to model snow accumulation and melt over a semi-arid mountain catchment. *Hydrological Processes* **16**(18), 3585–3603. doi: 10.1002/hyp.1238

Winstral A and Marks D (2014) Long-term snow distribution observations in a mountain catchment: assessing variability, time stability, and the representativeness of an index site. *Water Resources Research* **50**(1), 293–305. doi: 10.1002/2012WR013038